Journal of Alloys and Compounds 504 (2010) 265–272

Contents lists available at ScienceDirect

Journal of Alloys and Compounds

journal homepage: www.elsevier.com/locate/jallcom

Applying an electron counting rule to screen prospective thermoelectric alloys: The thermoelectric properties of $YCrB_4$ and Er_3CrB_7-type phases

J.W. Simonson*, S.J. Poon

Department of Physics, University of Virginia, 382 McCormick Rd., Charlottesville, VA 22904-4714, USA

ARTICLE INFO

Article history:
Received 5 March 2010
Received in revised form 13 May 2010
Accepted 21 May 2010
Available online 4 June 2010

Keywords:
Boride
Bonding
Gap formation
Thermoelectric
Electron counting

ABSTRACT

An electron counting rule, which was recently expanded to study molecular organometallics, boranes, and metallocenes, is utilized herein to predict the formation of a semiconducting gap or pseudo-gap in the density of states of deltahedral crystalline solids at or near the Fermi energy. It is suggested that this rule may be exploited to screen intermetallic compounds for prospective thermoelectric materials. The rule was applied to several structure types of known deltahedral boride and borocarbide compounds, and its predictions were compared to those of first principles electronic structure calculations when such were available in the literature or to published reports of transport properties. In addition, the rule has been used to predict the properties of several materials for which the electronic structure and properties have not hitherto been reported. In accordance with these predictions, layered ternary boride intermetallic compounds with structure types $YCrB_4$ and Er_3CrB_7 were synthesized, and the electrical resistivity and Seebeck coefficients of these alloys were measured from room temperature to 1100 K. Alloys of composition RMB_4 (R = Y, Gd, Ho; M = Cr, Mo, W) were found to be n-type semiconductors and to exhibit thermopower up to ~70–115 μV/K; the band gap was estimated to range from 0.17 to 0.28 eV, depending on composition. Undoped $YCrB_4$ was measured to have a maximum power factor of 6.0 μW/cm K^2 at 500 K and Fe-doped $YMoB_4$ of 2.4 μW/cm K^2 near 1000 K.

1. Introduction

Intermetallic borides are attractive materials for a wide variety of applications, largely due to their exceptional hardness, high melting points, and chemical inertness at elevated temperatures. In particular, the more boron rich phases have attracted interest as potential materials for extremely high temperature (even up to 2000 K) thermoelectric power generation [1–3], due to their high temperature stability and to the complexities of their structures, which often result in hopping electron conduction and low thermal conductivity at such elevated operating temperatures. These compositions tend to be dominated by boron sub-structures that are invariably electron poor, necessitating the interposition of metal electron donors for stability [4,5]. Boron is trivalent and therefore classically capable of forming only three 2c–2e covalent bonds, leaving the remaining valence orbital unfilled. For this reason, a covalent boron network must resort to multi-centre bonding via cluster formation in order to achieve stability. These B–B covalent networks take a wide variety of forms: from icosahedra, as in the structures of β-B [6], UB_{12} [7], $MgAlB_{14}$ [8], and many other more complicated structures; to octahedra, as in the cases of CaB_6 [9] and Th_2NiB_{10} [10]; to polygonal layers; and to derivatives thereof.

Immediately following the discovery of superconductivity to 39 K in MgB_2 [11] there was a dramatic surge in experimental and theoretical investigation into the subject of the magnetic and electronic properties of the diborides, the structure of which consists of alternating metal layers and graphite-like layers of hexagonal boron sheets. Over the years, several surveys have been published on the electronic structures and thermal properties of the transition metal diborides with the AlB_2 structure, and the existence of a pseudo-gap was found to be a common feature among the entire series [12,13]. The diborides of tetravalent transition metals were found to exhibit the greatest thermal stability, which corresponded with the prediction of electronic structure calculations that the Fermi energies of these compounds sat at or near the minimum of that pseudo-gap, while the Fermi energies of higher and lower group transition metal diborides were predicted to fall above or below the minimum of the pseudo-gap, respectively. Due to the absence of a pseudo-gap in isostructural YHg_2 and $HfBe_2$ and its presence in AlB_2, which certainly lacks any d-orbital hybridization, it was suggested that pseudo-gap formation is the result of multi-centre bonding within the B–B covalent network [10]. Moreover, this suggestion begs comparison to the somewhat analogous formation of the energy gap in the CaB_6 and UB_{12} systems, as was postulated by the symmetry-based electron counting models of the

* Corresponding author. Tel.: +1 434 924 6793; fax: +1 434 924 4576.
E-mail addresses: jws9n@virginia.edu, jwsimonson@gmail.com (J.W. Simonson).

0925-8388/$ – see front matter © 2010 Elsevier B.V. All rights reserved.
doi:10.1016/j.jallcom.2010.05.110

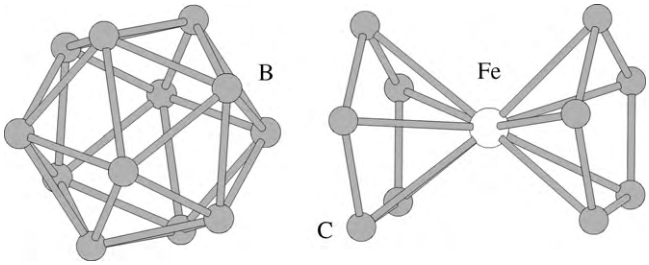

Fig. 1. Icosahedral borane molecule (left) and ferrocene molecule (right). The Fe atom is white, and the B or C atoms are gray. H atoms are omitted for clarity but are located radially outward from the B and C atoms.

early investigators of these compounds [4,5], i.e. that the so-called bonding orbitals of the polyhedral boron unit are fully occupied, the non-bonding orbitals are half occupied, and the anti-bonding orbitals are wholly unoccupied. The determination of the bonding nature of each orbital and the relative location of the HOMO–LUMO gap, however, is in general a nontrivial problem, and has only been solved analytically in the highest symmetry cases, those of the full icosahedral and full octahedral point groups [5,9].

To address the lack of a formal solution to the bonding scheme of more complex systems, a set of electron counting rules, commonly referred to as Wade's rules, was developed in the 1970s to predict the formation of new molecular structures and to determine the stability of polyhedral boranes via the method of molecular orbitals [14]. In the past decade, Wade's rules for assigning electron occupancy to simple boron sub-clusters have been subsequently generalized to include macro-polyhedral boranes, metallocenes, and organometallic molecules under the heading of the so-called "*mno* rule" [15]. The "*mno* rule" postulates that the number of occupied molecular orbitals, N, in a cluster with deltahedral geometry – such as a borane or carborane – is given by the sum of m, n, and o, where m is the number of polyhedra in the cluster, n is the number of vertices, and o is the number of single-vertex-sharing condensations. The more familiar Wade $n+1$ rule merely treats a special case with one polyhedron ($m=1$) and no condensations ($o=0$). As an example, consider the single icosahedral borane molecule in Fig. 1, in which a boron atom is located on each vertex of a regular icosahedron with a covalently bonded hydrogen atom oriented radially outward. Such a cluster is referred to as *closo* or "closed" to signify that it lacks no deltahedral vertices. In this example, the molecular unit includes one polyhedron, twelve vertices, and no condensations, yielding $N=1+12+0=13$ orbitals below the HOMO–LUMO gap. Some 26 electrons are therefore required for stability, but only 24 are available; each of the 12 boron atoms provides two electrons to skeletal bonding while their remaining electron is dedicated to the formation of a 2c–2e classical covalent bond with hydrogen. As a result, two additional electrons are needed for structural stability of the cluster. It bears mention that this result is identical to that obtained from the computationally rigorous Longuet–Higgins' technique, which results in the analytical solution of the energies of the borane molecular orbitals in the I_h point group [5].

For an example more appropriate to the discussion of bulk layered borides, consider the sandwich molecule ferrocene in Fig. 1 – the structure of which consists two co-parallel open (so-called *nido* to signify the lack of one vertex) cyclopentadienyl (C_5H_5) rings located on opposite sides of a central condensed vertex occupied by an iron atom. In this case, there are two polyhedra, a total of eleven occupied vertices including that of iron, one condensation at the iron site, and two unoccupied vertices, yielding $N=2+11+1+2=16$. Each carbon atom contributes three electrons to the total count, and as is analogous to the boron case above, the fourth is bonded with hydrogen. A covalently bonded iron atom contributes two electrons, for a total of 32 electrons, perfectly filling those orbitals below the HOMO–LUMO gap and providing insight into why $Fe(C_5H_5)_2$ is stable while other isostructural cyclopentadienyl complexes such as chromocene or cobaltocene are far more reactive due to a lack of electrons or the occupation of anti-bonding states, depending on the metal atom.

With Jemmis' *mno* rule able to predict the stability of stability of macro-polyhedral molecules with high accuracy, only a few steps must be taken to apply this construction to bulk intermetallic compounds. It is well known that stability in a molecular system is achieved by filling molecular orbitals to the brink of the HOMO–LUMO gap. Therefore the assumption is made herein that an equivalent situation occurs in a crystalline solid when a sufficient number of electrons serves to position the Fermi energy exactly at the cusp of a band gap or pseudo-gap. A validation of this assumption is presented in Section 4 of this work via comparison of the predictions of an electron counting rule for bulk compounds with the results of published electronic structure calculations and transport measurements. This generalized *mno* rule is shown to provide a simple and easy-to-use tool to enable quick screening of potential thermoelectric materials that fit the necessary structural motif and to offer a gateway into explanation of their electronic properties. The alloys presented in this work are an example of the results of such a screening.

It is important to note, however, that the expansion of electron counting rules from molecules to crystalline solids is far from a novel idea in general. Indeed, even a book has been recently published on the subject, addressing several methods of counting skeletal electron pairs and cluster valence electrons. The book also covers the generalization of these molecular orbital models to crystalline systems either by examination of cluster analogues or via the Zintl-Klemm concept [16]. A more in depth discussion of Wade's rule for molecular and cluster systems, as well as of *closo*, *nido*, and *arachno* boranes is presented in its early chapters. Of particular relevance to the bonding of crystalline borides is the discussion of the stability of the rare earth hexaborides and of GdB_4, neither of which can be explained by naive application of the Zintl-Klemm approach. In addition to that text, during the review process for this article, the authors of the present work were made aware of a recent publication that outlines the relationship between electron and valence counting rules and the structural arrangements and stabilities of cluster, chain, and ring compounds, including the layered borides $YCrB_4$, $ThMoB_4$, and Y_2ReB_6 [17]. Rather than using the *mno* rule as a starting point, the article discusses the bonding of such systems via consideration of several possible oxidation numbers of the boron networks and the critical examination of electronic structure calculations based on these possible states. Overall, the methods of generalization presented in these two sources offer insight into the bonding of boron- and carbon-based compounds that is complementary to what can be learned by the procedure described in the remainder of this article.

As mentioned above, there has been a great deal of work published on transitional metal diborides, but several ternary alloys with similar structures have not yet been as thoroughly investigated. The current study of electron counting in some of these systems, however, has suggested their potential for thermoelectric application. Consider for example the $YCrB_4$-type compounds. While the structure of AlB_2 consists of alternating layers of metal atoms and boron hexagons, the boron network of the $YCrB_4$ structure type is instead built of pentagons and heptagons to accommodate metals of varying sizes [18]. It forms for over 100 different compositions [19]. LMTO calculations performed as part of an ongoing search for superconductivity in layered borides have shown $YCrB_4$ in particular to be a semiconductor with a narrow band gap of about 0.05 eV, with the states near the gap being of predominantly Cr-d character and with significant d-orbital hybridization [20]. More recently, alloys with the $YCrB_4$ structure

have been investigated for their interesting physical and magnetic properties [19,21]. Furthermore, a somewhat related structure type has received less attention. The Er_3CrB_7 structure, first synthesized by the same group, has corrugated metal layers and corrugated layers of boron pentagons and irregular polygons [22]. In this work, the generalized *mno* rule is applied to both these structure types and is suggestive of gap formation near the Fermi energy. Accordingly, the thermopower and electrical resistivity of alloys of these two structure types was measured from room temperature to 1100 K, and the results are discussed in terms of the generalized *mno* electron counting model.

2. Experimental procedure

Polycrystalline ingots of RMB_4 (R = Y, Gd, Ho, Er, Yb; M = Cr, Mo, W) and Y_3MB_7 (M = Cr, Mo, Fe) were formed by arc melting high-purity pieces (greater than 99.9%) of the constituent elements under a flowing argon atmosphere. Each ingot was flipped and subsequently remelted at least four times in the arc furnace to ensure a homogeneous composition in the final ingot. Mass losses during arc melting were confined to less than 1% of the initial mass. Ingots containing Yb were made by adding 5% excess Yb to a MB_4 precursor to compensate for evaporative losses. Ingots of $YMoB_4$ were prepared with either 20% Fe in place of Mo or 5% C in place of B to study the effects of dopants on the electronic properties. The expected crystal structure and purity of each phase was confirmed by performing two-circle powder x-ray diffraction with Cu Kα radiation. Ingots were cut into rectangular blocks of dimension 2 mm × 2 mm × 10 mm for measurement. Nearly simultaneous measurements of electrical resistivity and Seebeck coefficient were made under vacuum from room temperature to 1100 K and back over a 6-h period. Electrical resistivity was measured via the DC four-point technique with silver leads, while thermopower was measured by the differential method using chromel–alumel thermocouples attached by pressure contact as described elsewhere [23]. Each measurement of the Seebeck coefficient was calculated from a linear best fit routine performed on between 40 and 60 temperature and voltage differences. Carrier concentrations were determined from Hall measurements that were performed on a Quantum Design PPMS.

3. Results and discussion

3.1. The mno rule and bulk compounds

A few paragraphs will now be devoted towards explaining the framework for generalizing Jemmis' *mno* to bulk compounds. While the generalization of molecular electron counting rules to crystalline solids is certainly not a new idea, the following procedure is convenient because it requires only an understanding of the crystal structure of the material, which is frequently the first detail reported when a new compound is found. Thus, no knowledge of possible oxidation numbers or molecular bonding orbital configurations is necessary to obtain some information about the density of states near the Fermi energy.

As such, to extend Jemmis' *mno* rule from the molecular domain to that of bulk materials requires several steps. First, an appropriate section of the bulk material must be selected for counting of polyhedra and vertices, which is analogous to the comparison made between molecular clusters and crystalline solids in Ref. [16]. In general, the contents of this selection must be equivalent to the crystallographic unit cell, but the *mno* rule is most elegantly applied to a section that is clearly parallel to a molecular construction, i.e. one in which each polyhedron of the structure can be identified and completely contained. Fig. 2 shows the selection of an appropriate section of the $YCrB_4$ structure, which like the unit cell contains four heptagonal bi-pyramids and four pentagonal bi-pyramids. Unlike the unit cell, however, the x and y axes have been shifted by 50% and 40% of their respective lattice vectors to move these deltahedral structures away from arbitrarily straddling the edges of the unit cell.

Second, because the external vertices of the selected structure are not conveniently capped with hydrogen atoms as was the case with the molecular examples above, special care must be taken not to double-count vertices. Each metal atom at the zenith and

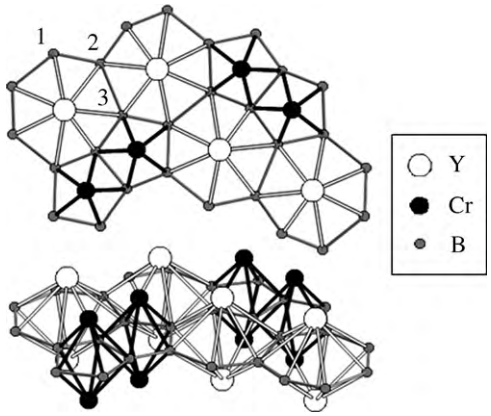

Fig. 2. The $YCrB_4$ crystal structure – viewed down the *z*-axis (top) and 30° above the *x*–*y* plane (bottom) – equivalent to the unit cell but shifted to prevent deltahedra from straddling the boundary. Yttrium bonds and atoms are represented as white, chromium as black, and boron as gray.

the nadir of a single bi-pyramid is located at a crystallographically equivalent position. Thus each only counts as half a vertex; it is in effect shared with the adjacent identical structure in the positive or negative *z* direction. Likewise, each boron atom is shared by three separate deltahedra. Depending on the boron atom in question, one, two, or all three of these deltahedra may be contained within the selected section. An example of each boron configuration is marked in Fig. 2; boron atom number one is part of one deltahedron in the selected structure and two in adjacent structures. Likewise, boron atom number two is also shared by three deltahedra, two of which are located within the selection. An analogous but more obvious argument can be made for boron atom number three, which is entirely a member of the selected section. To avoid double-counting, shared atoms must be counted fractionally in all cases when considering vertices, condensations, and electrons donated to the structure. Overall, there are 16 B atoms, four Cr atoms, and four Y atoms in the selected structure, yielding a total of 24 atoms.

Proceeding with the example of the $YCrB_4$-type compounds, the selected structure in Fig. 2 contains eight polyhedra – four each of heptagonal and pentagonal bi-pyramids – yielding $m = 8$. Like boron atom number 3, some six boron atoms are wholly contained in this structure, while eight are members of two selected polyhedral and one external polyhedron, and 14 are members of only one selected polyhedron. These boron atoms contribute an entire vertex, two-thirds of a vertex, and one-third of a vertex, respectively. In addition, the 16 metal atoms each contribute half of a vertex and half of a condensation due to the fact that each is shared with the neighboring section of the next higher or lower layer. In sum, the selected structure contains 24 vertices ($n = 6 + 8 \times 2/3 + 14 \times 1/3 + 16 \times 1/2 = 24$) and 8 condensations ($o = 16 \times 1/2$). In molecular parlance, the total number of orbitals below the HOMO–LUMO gap is 40 ($N = 8$ polyhedra + 24 vertices + 8 condensations = 40). Division of electrons is determined by an identical method; each of the four half-shared Y atoms contributes 1.5 electrons, each half-shared Cr contributes 3, and each boron contributes between 1 and 3, depending on how many of its parent deltahedra are contained within the selection. For the example composition of $YCrB_4$ this total comes to 84 electrons, which slightly overfills the 40 *mno* orbitals. Thus, there is an excess of 0.17 electrons per atom for each molecular unit.

Table 1 lists the results of application of the *mno* rule to several icosahedral, octahedral, and layered bulk structures and a comparison of these results to published electronic structure calculations or measurements when such work is available in the literature. In gen-

Table 1
Application of the *mno* rule to bulk materials.

Composition	Structure	*mno* capacity/unit cell	e^-/unit cell	e^- excess/atom	Published result	Ref.
$Er_{0.62}Al_{0.73}B_{14}$	Icosahedral	23 orbitals	46	0	Semiconductor	[26]
CaB_6	Octahedral	10 orbitals	20	0	Semiconductor	[9]
KB_5C	Octahedral	10 orbitals	20	0	Semiconductor	[27]
MgB_2C_4	Layered	12 orbitals	24	0	Semiconductor	[28]
CaB_2C_2	Layered	8 orbitals	16	0	Semiconductor	[25]
TiB_2	Layered	5 orbitals	10	0	Pseudo-gap at E_F	[13]
YB_2C	Layered	26 orbitals	52	0	Pseudo-gap at E_F	[29]
$YCrB_4$	Layered	40 orbitals	84	0.17	Semiconductor	[20]
Y_2NiB_{10}	Octahedral	19 orbitals	46	0.62	Metallic	[30]
WB_4	Layered	15 orbitals	34	0.40	Metallic	[31]
Y_2ReB_6	Layered	60 orbitals	124	0.11	Metallic	[20]
Y_3CrB_7	Layered	34 orbitals	72	0.18	Unreported	[22]
Pr_2B_5	Layered & Octahedral	62 orbitals	120	−0.07	Unreported	[32]
$ErMoB_3$	Layered	16 orbitals	36	0.40	Unreported	[33]
YMo_3B_7	Layered	32 orbitals	84	0.91	Unreported	[33]

eral, there is a direct correlation between the complete filling of the *mno* orbitals with electrons and the presence of a semiconducting gap or pseudo-gap in the density of states at the Fermi level. Moreover, it is readily apparent that addition or subtraction of electrons from an *mno*-satisfied system will result in metallic behavior: YB_6, isostructural with semiconducting CaB_6 is metallic and superconducting below 8.4 K [24]; density of states calculations performed on YB_2, VB_2, and CrB_2 – all isostructural with TiB_2 – reveal the Fermi level to be above or below the pseudo-gap as the number of valence electrons increases or decreases [13]; and YB_2C_2, isostructural with semiconducting CaB_2C_2, is metallic and superconducting below 2.2 K [25]. Along these lines, this application of the *mno* rule also appears to have some utility in predicting the appearance of gaps or pseudo-gaps in the density of states that are some distance away from the Fermi energy. The density of states of WB_4, for example, is reported to contain a pseudo-gap approximately 3 eV below the Fermi energy [31]. One might therefore speculate that if it were possible to adjust the composition of a WB_4 structure-type material to remove the 0.40 electron/atom excess predicted in Table 1, that the Fermi energy would fall at the minimum of that pseudo-gap, potentially resulting in a material with even greater thermal stability, a situation analogous to that seen with TiB_2 [13].

Notably, the $YCrB_4$ structure is one of the few structures examined in which there is an overfilling of the *mno* orbitals but the material is nonetheless a semiconductor. This behavior may be due to incomplete electron transfer from transition metal to boron or more likely to a greater degree of overlap and hybridization of the d-orbitals when compared with the simpler MB_2 structure, in part caused by a greater number of d-metal electrons and shorter inter-transition metal distances. The Cr–Cr distance is 2.97 Å in the hexagonal AlB_2 structure, while Cr atoms capping the smaller pentagonal bi-pyramids of $YCrB_4$ are only separated by 2.38 Å, a relative decrease of 20% [18,34]. In either case, even if the *mno* rules lack the ability to predict the formation of additional bonding states created by d–d orbital hybridization, their accuracy in predicting the electronic properties of alkali metal, alkali earth, and rare earth borides and borocarbides – cases in which the atomic energy levels are sufficiently above the energy levels of the boride clusters and d–d orbital hybridization is not an issue – remains high. Moreover, even in alloys that contain higher valent transition metals, saturation of the *mno* orbitals provides a strong indication of an important feature in the density of states near the Fermi energy. Take for example Y_2ReB_6, which nearly satisfies the *mno* rule and features a pseudo-gap approximately 1 eV above the Fermi energy. It is particularly noteworthy that compounds with a small excess or deficiency of electrons are nevertheless candidates for semiconducting behavior in the presence of d-orbital hybridization even if d-orbital hybridization alone will not open a gap.

In addition to materials for which the electronic structure is already known, this method of electron counting was applied to several compounds for which there has been no published report of electronic structure calculations or transport properties. While compounds with the Y_3CrB_7 structure were found not to satisfy this rule exactly, they were nonetheless selected for further investigation in this work due to what was judged to be the likelihood of transition metal d–d orbital hybridization contributing to the opening of a gap at the Fermi energy as appears likely to be the underlying cause of the gap in the $YCrB_4$-type compounds. The recently reported Pr_2B_5 compound, however, was not selected for further investigation, despite its relatively small electron deficiency. In this case, the procedure of electron counting again resulted in the prediction of metallic behavior, but the chance of opening a gap via Pr-d hybridization was expected to be minimal. Likewise, the electron excess per atom of the $ErMoB_3$ and YMo_3B_7 structures was in each case sufficiently large to preclude those materials from further consideration for thermoelectric application, notwithstanding their complex structures.

3.2. Structural verification

Two-circle powder X-ray diffraction was performed to verify both the formation of the expected phases and the inclusion of dopants into the crystal structure when relevant. Diffraction scans were compared to patterns calculated from lattice constants and atomic parameters reported in the literature [18,22]. An example of a measured diffraction pattern is shown in Fig. 3, in this case the pattern of $YMo_{0.8}Fe_{0.2}B_4$, and displays no additional peaks beyond those of the $YCrB_4$ phase. Furthermore, no substantial change in the lattice parameter was produced by the substitutional doping. Similar scans were performed on the other alloys reported in this work to verify the formation of single phased ingots.

3.3. Transport properties of $YCrB_4$-type alloys

It is well know that a wide, sharp gap or pseudo-gap in the vicinity of the Fermi energy is advantageous for a high Seebeck coefficient. In accordance with the prediction that $YCrB_4$ is a semiconductor [20] and the near-satisfaction of the *mno* rule, alloys of this structure type were selected for synthesis and characterization of thermoelectric properties. Fig. 4 shows measurements of the thermopower and electrical resistivity of YMB_4 for M = Cr, Mo, W from room temperature to 1100 K. These measurements confirm that all three compositions are narrow gap semiconductors, as was predicted by Medvedeva's density of states calculation of $YCrB_4$.

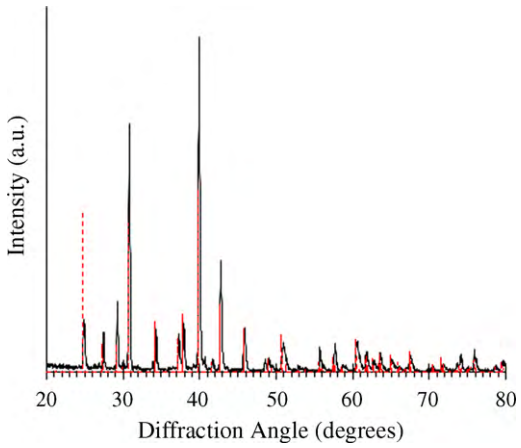

Fig. 3. X-ray diffraction measurement of $YMo_{0.8}Fe_{0.2}B_4$ displaying complete dopant inclusion into the $YCrB_4$ structure. The solid black curve displays the results of the measurement, and the red dashed lines are calculated from the lattice constants and atomic parameters given in Ref. [18]. (For interpretation of the references to color in this figure legend, the reader is referred to the web version of the article.)

To this end, the slopes of logarithmic plots of the high temperature end of the resistivity curves (from 900 to 1100 K) were plotted on a logarithmic scale and analyzed according to the well-known relation for activated behavior in semiconductors, which has previously been applied to the study of thermoelectric materials [35]:

$$\rho \sim \exp\left(\frac{\varepsilon_g}{2k_B T}\right),$$

where ρ is the electrical resistivity and ε_g is the width of the band gap. The results are presented in Fig. 4. At these sufficiently high temperatures, the logarithmic resistivity plots become linear, and the resulting slopes were used to estimate the width of the band gaps of these alloys. $YCrB_4$ was estimated to have a gap width of 0.17 eV. Although the measured band gap value is significantly higher than the reported calculation of 0.05 eV [20], it is not unreasonable if one takes into account the tendency of LDA calculations to underestimate the band gap of semiconductors. A gap of 0.28 eV is obtained for $YMoB_4$. No such analysis was possible for YWB_4, due to the non-linear behavior of the logarithmic resistivity points across the highest temperature regime measured, which is likely a result of the high Debye temperature of the tungsten-containing alloy. Despite the fact that these compounds and the others presented in this work were synthesized as polycrystalline ingots, the quality of the materials is shown to be more than sufficient to distinguish semiconducting and metallic behavior, even if the existence of defects or imperfections results in higher order adjustments to the Seebeck coefficient or electrical resistivity when compared to what might be expected for a single crystal material.

Thermopower is of moderately high n-type character across the board, which may be indicative of the slight electron excess predicted by the generalized *mno* counting rules. The more robust thermopower of $YMoB_4$ at elevated temperatures, compared with that of $YCrB_4$ is consistent with the larger band gap estimate of the former composition, as is the latter compound's significantly lower resistivity. Furthermore, the thermopower rollover in YWB_4 is located near 900 K, much higher than the rollover of the other two compounds, pointing to a wider gap as well. In short, the increase in metallic radius from Cr to Mo or W appears to have a systematic widening influence on the size of the gap. These effects may be due to increased d–d orbital overlap and stronger orbital hybridization. The results of power factor calculations of the undoped YMB_4 alloys are modest, which is attributed to the moderate thermopower but comparatively high resistivity of these compounds. The power factor of $YCrB_4$ reaches 6.0 μW/cm K^2 at 500 K even if it rolls over at a relatively low temperature.

In addition to isoelectronic transition metal substitution, attempts were made to study the effects of the size of the rare

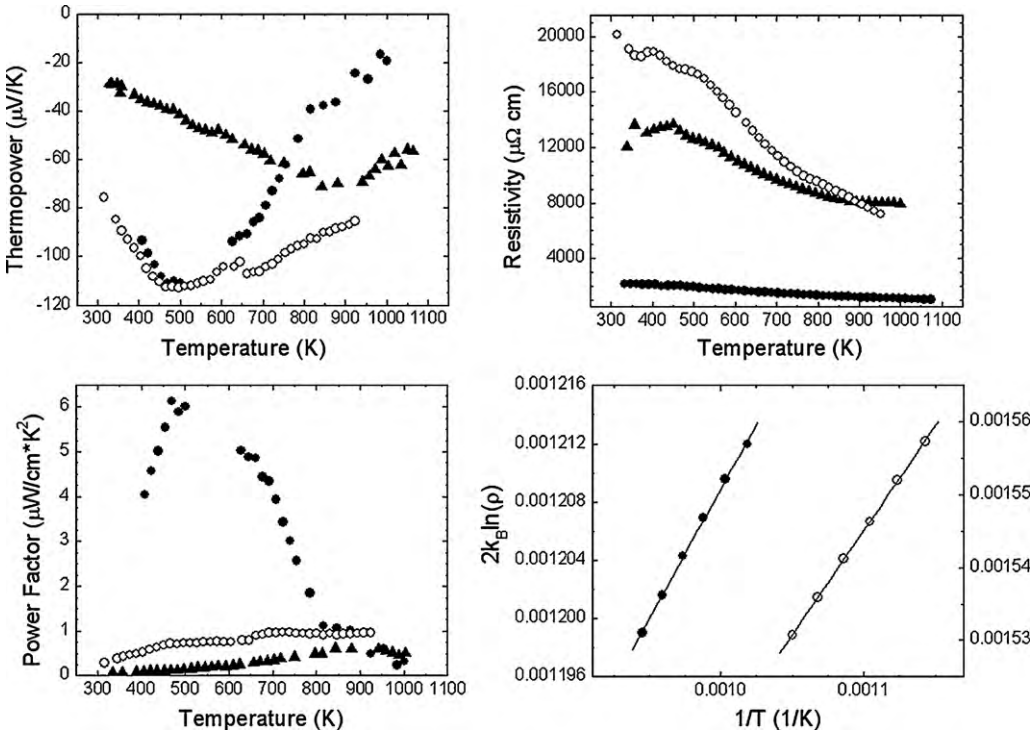

Fig. 4. High temperature thermopower, electrical resistivity, and power factor measurements of YMB_4 (M = Cr, Mo, W). The black circles represent $YCrB_4$, the white circles $YMoB_4$, and the black triangles YWB_4. The lower right panel displays the line fits used to estimate band gaps for $YCrB_4$ and $YMoB_4$ from high temperature electrical resistivity trends.

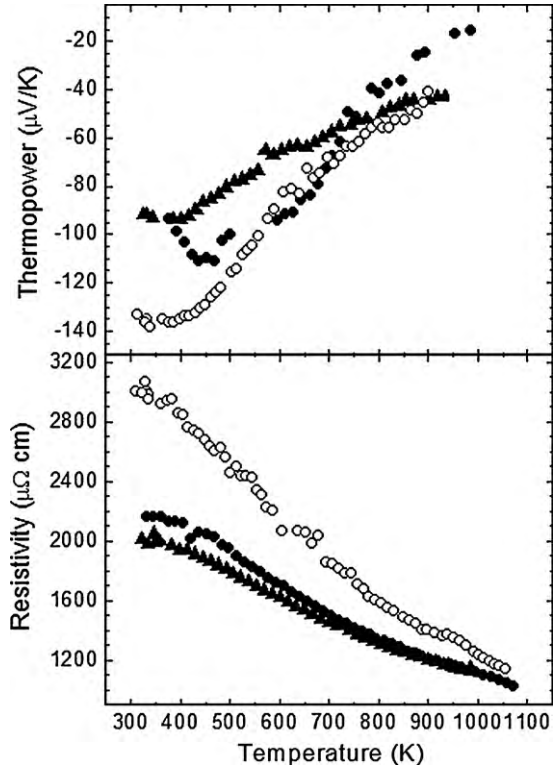

Fig. 5. High temperature thermopower and resistivity measurements of $RCrB_4$ (R = Y, Gd, Ho). The black circles represent $YCrB_4$, the white circles $GdCrB_4$, and the black triangles $HoCrB_4$.

earth element in the $YCrB_4$ structure on the transport properties. Fig. 5 includes plots of the thermopower and electrical resistivity of $RCrB_4$ for R = Y, Gd, and Ho. It is clear from the figure that substitution of rare earth elements to the Y site produces only minor changes in the electronic properties compared with those produced by even isoelectronic transition metal substitution. In particular, both the electrical resistivity and thermopower measurements of the different compositions approach convergence at elevated temperatures. Either the size difference between Y, Gd, and Ho is too small to produce a noticeable effect at these temperatures, or a systematic decrease in rare earth element size has little to do with the electronic structure near the gap.

Given that the electronic properties of these alloys have been understood from a band-filling perspective, dopant atoms were introduced to add additional carriers in hopes of improving thermoelectric performance. N-type dopants were selected for two reasons: first, that transition metals to the left of the chromium group on the periodic table are not able to inhabit the higher valent transition metal site in the $YCrB_4$ structure, largely due to size constraints, and second, that the intrinsic n-type thermopower might be enhanced by the substitution. Carbon was selected as a dopant due to its chemical similarity to boron and its ease of inhabiting equivalent lattice positions in layered borocarbides such as YB_2C, MgB_2C_4, and CaB_2C_2. Fig. 6 shows the effects of dopants on the $YMoB_4$ system. In both cases of replacement of 5% of B with C and 20% substitution of Fe to the Cr site, the doping is found to be efficient, resulting in significantly lowered resistivity across the entire temperature spectrum. Furthermore, in the case of Fe substitution, the thermopower values do not rollover until a significantly higher temperature is reached, likely due to the addition of extra n-type carriers to the conduction band to compensate the deleterious effects upon the Seebeck coefficient of thermally activated minority conduction through the valence band. These data are in agreement with an increase in carrier concentration from

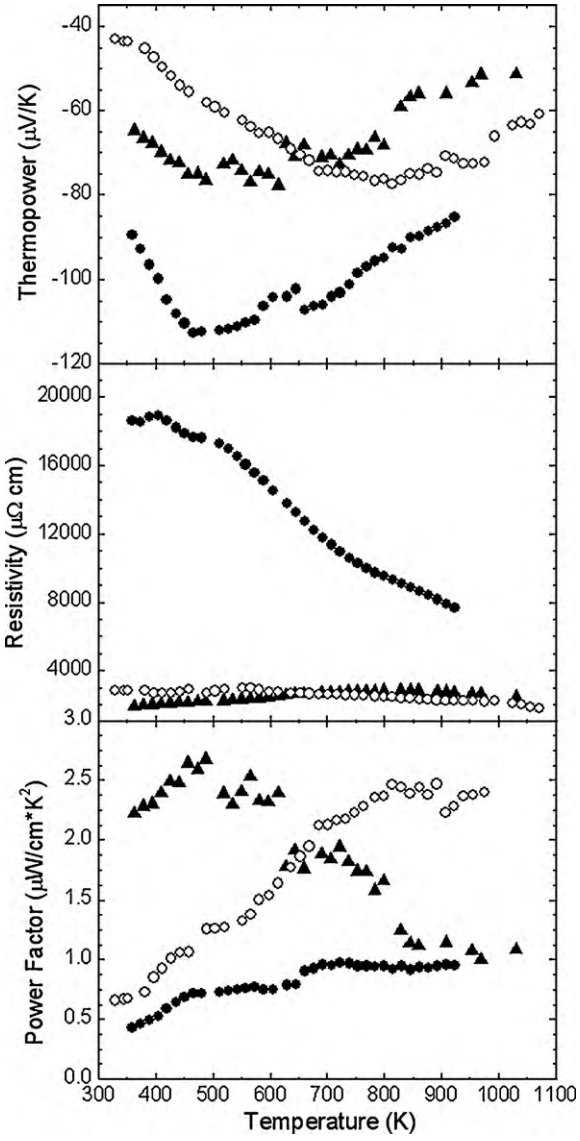

Fig. 6. High temperature thermopower, electrical resistivity, and power factor measurements of doped $YMoB_4$. The black circles represent $YMoB_4$, the white circles $YMo_{0.8}Fe_{0.2}B_4$, and the black triangles $YMoB_{3.8}C_{0.2}$.

$3.5 \times 10^{19}\,cm^{-3}$ for undoped $YMoB_4$ to $2.1 \times 10^{20}\,cm^{-3}$ with 20% Fe doping. In this composition in particular, the power factor is improved by a factor of 2.5 compared to the undoped alloy to a maximum of $2.4\,\mu W/cm\,K^2$ near 1000 K and remains nearly level over a range of 200 K, as the electrical resistivity is greatly diminished with only slight losses in thermopower. Thus, the magnitude of the thermoelectric figure of merit ZT is expected to increase further with optimization of dopant species and amount and with measurement to higher temperatures. The thermal conductivity measurements necessary to calculate ZT, however, were not performed in this work. Simply put, although the power factors of these compounds compare favorably with those reported for other borides, they fall far short of those of state-of-the-art non-boron-based thermoelectric compounds, making thermal measurements unnecessary.

3.4. Transport properties of Er_3CrB_7-type alloys

The existence of the Er_3CrB_7 structure type was published over 20 years ago [22], and yet there have been no publications of band

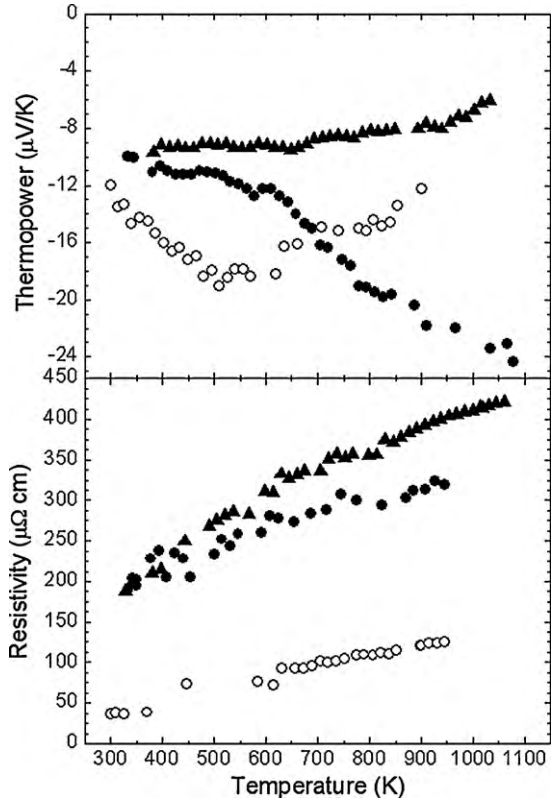

Fig. 7. High temperature thermopower and electrical resistivity of Y_3MB_7 (M = Cr, Mo, Fe). The black circles represent Y_3CrB_7, the white Y_3FeB_7, and the black triangles Y_3MoB_7.

structure calculations or electronic properties to the knowledge of this author. The Er_3CrB_7 structure – composed of corrugated layers of boron pentagons and open structures that resemble triply merged heptagons – is remarkably similar to the layered pentagonal and heptagonal bi-pyramids of the $YCrB_4$ structure. Moreover, according to Table 1, the *mno* counting rules predict a similar electron excess per atom. Given these similarities and the favorable but modest thermoelectric performance of the $YCrB_4$-type compounds, Y_3CrB_7, Y_3MoB_7, and Y_3FeB_7 were synthesized and their properties measured to determine if any composition would display semiconducting properties. The results are displayed in Fig. 7 and indicate that all three compositions are low thermopower metallic alloys. Whether these properties can be attributed to the formation of a non-zero density of states within the gap or to the Fermi energy lying at some point distant from that gap is unfortunately beyond the scope of the generalized *mno* rule and therefore cannot be determined without further investigation, such as first principles electronic structure calculations.

4. Conclusions

When viewed in light of band structure calculations and experimental measurements, a form of the *mno* counting rules – originally intended to predict the structural stability of molecular deltahedral complexes – has proven apt in providing insight into the electronic structure of certain bulk crystalline solids. Specifically, it has been shown that the formation of a band gap or pseudo-gap at the Fermi energy can be predicted in borides and borocarbide intermetallic compounds that contain alkali metals, alkali earth metals, rare earth metals, or lower valent transition metals, provided a deltahedral bonding motif is satisfied. Boride compositions that contain higher valent transition metals, however, may be more susceptible to the effects of d–d orbital hybridization, in effect stabilizing a slightly greater number of orbitals below the gap than is predicted by electron counting. The onset of d–d orbital hybridization, in particular, is likely the root cause of the semiconducting properties of the $YCrB_4$-type alloys, providing a sharp distinction from the band-filling models that explain the origin of a gap at the Fermi energy in CaB_6, $Er_{0.62}Al_{0.73}B_{14}$, MgB_2C_4, and other closely related compounds. It is for this same reason that the electron counting scheme does not differentiate between semiconducting systems in which the density of states within the gap is truly zero and those which possess only a pseudo-gap at the Fermi level. Nevertheless, it is postulated that it may find utility in predicting features of the electronic structure of intercalated graphene compounds and related novel materials, due to the similar geometry and bonding trends between the layered borides and those systems.

This article displays the results of efficiently screening potential structures for thermoelectric application. The thermoelectric properties of the $YCrB_4$ family of compounds are reported with modest results that are nonetheless comparable to those of potential boride thermoelectric materials reported by other groups. Despite the fact that the doping of these alloys has not yet been optimized, Fe-doped $YMoB_4$ in particular possesses a power factor of 2.4 $\mu W/cm\,K^2$ at temperatures near 1000 K and remains nearly level even at the highest temperature measured. In addition, the application of a generalized form of the *mno* rule has suggested that certain compounds with unreported electronic structures and transport properties – such as Pr_2B_5, $ErMoB_3$, and YMo_3B_7 – are unlikely candidates for further thermoelectric study.

Acknowledgements

The authors wish to thank M.J. Pierotti for his assistance with sample preparation and alloying and M.A. Commisso for her assistance with the Hall measurements.

References

[1] K. Yagasaki, S. Notsu, Y. Shimoji, T. Nakama, R. Kaji, T. Yokoo, J. Akimitsu, M. Hedo, Y. Uwatoko, Physica B 329-333 (2003) 1259–1260.
[2] T. Mori, J. Appl. Phys. 97 (2005) 093703.
[3] T. Mori, T. Nishimura, Proc. Int. Conf. Thermoelect. (2006) 164–167.
[4] H.C. Longuet-Higgins, M.V. Roberts, Proc. R. Soc. A 230 (1955) 110.
[5] D.W. Bullett, J. Phys. C 15 (1982) 415–426.
[6] J.L. Hoard, D.B. Sullenger, C.H.L. Kennard, R.E. Hughes, J. Solid State Chem. 1 (1970) 268–277.
[7] Y. Imai, M. Mukaida, M. Ueda, A. Watanabe, Intermetallics 9 (2001) 721.
[8] M.M. Korsukova, V.N. Gurin, Y.B. Kuzma, N.F. Chaban, S.I. Chykhrii, V.V. Moshchalkov, N.B. Brandt, A.A. Gippius, K.K. Nyan, Phys. Stat. Sol. A 114 (1982) 265.
[9] H.C. Longuet-Higgins, M.V. Roberts, Proc. R. Soc. Lond. 224 (1954) 336.
[10] W. Jeitschko, T. Konrad, K. Hartjes, A. Lang, R.D. Hoffmann, J. Solid State Chem. 154 (2000) 246.
[11] J. Nagamatsu, N. Nakagawa, T. Muranaka, Y. Zenitani, J. Akimitsu, Nature (London) 410 (2001) 63.
[12] J.K. Burdett, E. Canadell, G.J. Miller, J. Am. Chem. Soc. 108 (1986) 6561–6568.
[13] P. Vajeeston, P. Ravindran, C. Ravi, R. Asokamani, Phys. Rev. B 63 (2001) 045115.
[14] K. Wade, Adv. Inorg. Chem. Radiochem. 18 (1976) 1–66.
[15] E.D. Jemmis, M.M. Balakrishnarajan, J. Am. Chem. Soc. 123 (2001) 4325.
[16] T.P. Fehlner, J.-F. Halet, J.-Y. Saillard, Molecular Clusters: A Bridge to Solid State Chemistry, Cambridge University Press, 2007.
[17] S. Lassoued, R. Gautier, A. Boutarfaia, J.-F. Halet, J. Organomet. Chem. 695 (2010) 987–993.
[18] B. Kuz'ma Yu, Sov. Phys. Crystallogr. 15 (1970) 312–314.
[19] I. Veremchuk, T. Mori, Yu. Prots, W. Schnelle, A. Leithe-Jasper, M. Kohout, Yu. Grin, J. Solid State. Chem. 181 (2008) 1983–1991.
[20] N.I. Medvedeva, E. Medvedeva, A.L. Ivanovskii, Dokl. Phys. Chem. 383 (2001) 75–77.
[21] T. Mori, H. Borrmann, S. Okada, K. Kudou, A. Leithe-Jasper, U. Burkhardt, Yu. Grin, Phys. Rev. B 76 (2007) 064404.
[22] B. Kuz'ma Yu, S.I. Mykhalenko, L.G. Akselrud, J. Less Common Metals 117 (1986) 29–35.
[23] S.R. Culp, S.J. Poon, N. Hickman, T.M. Tritt, J. Blumm, Appl. Phys. Lett. 88 (2006) 042106.
[24] R. Lortz, Y. Wang, U. Tutsch, S. Abe, C. Meingast, P. Popovich, W. Knafo, N. Shitsevalova, B. Paderno Yu, A. Junod, Phys. Rev. B 73 (2006) 024512.

[25] X. Rocquefelte, S.E. Boulfelfel, M.B. Yahia, J. Bauer, J.Y. Saillard, J.F. Halet, Angew. Chem. Int. Ed. 44 (2005) 7542–7545.
[26] H. Werheit, U. Kuhlmann, G. Krach, I. Higashi, T. Lundstrom, Y. Yu, J. Alloys Compd. 202 (1993) 269–281.
[27] B. Albert, K. Schmitt, Chem. Mater. 11 (1999) 3406–3409.
[28] C.-M. Fang, et al., J. Solid State Chem. 180 (2007) 2465–3247.
[29] J. Bauer, J. Debuigne, J. Inorg. Nucl. Chem. 37 (1975) 2473–2476.
[30] W. Jeitschko, T. Konrad, K. Hartjes, A. Lang, R.D. Hoffmann, Solid State Chem. 154 (2000) 246–253.
[31] M. Wang, Y. Li, T. Cui, Y. Ma, G. Zou, Appl. Phys. Lett. 93 (2008) 101905.
[32] B. Kuz'ma Yu, V.S. Babizhetskii, R. Guerin, S.I. Mikhalenko, Crystallogr. Rep. 48 (2003) 568–572.
[33] S.I. Mikhalenko, N.F. Chaban, B. Kuz'ma Yu, Powder Metall. Metal Ceram. 37 (1998) 99–106, and references therein.
[34] A. Raman, Z. Metallk. 58 (1967) 179–184.
[35] F.G. Aliev, N.B. Brandt, V.V. Moshchalkov, V.V. Kozyrkov, R.V. Skolozdra, A.I. Belogorokhov, Z. Phys. B - Condens. Matter 75 (1989) 167.